Experimental study on flame length and pulsation behavior of n-heptane continuous spill fires on water

Jinlong Zhao[a,b*], Guangheng Song[a], Qingyuan Zhang[a], Xinjiang Li[a],
Hong Huang[c], Jianping Zhang[d]

[a]*School of Emergency Management & Safety Engineering, China University of Mining & Technology, Beijing 100083, China*

[b]*National Academy of Safety Science and Engineering, MEM, China*

[c]*Institute of Public Safety Research, Department of Engineering Physics, Tsinghua University, Beijing 100084, China*

[d]*FireSERT, Belfast School of Architecture and the Built Environment, Ulster University, Newtownabbey, BT37 0QB, United Kingdom*

Abstract

Continuous spill fires pose significant risks to the storage and transportation industries of liquid fuels. To investigate the flame length and pulsation behavior of continuous spill fires, large-scale spill fire experiments were conducted on water to simulate the burning fuel on a water surface that could occur during firefighting of tank fires or due to leaked fuels on water during transportation, with varying discharge rates (3, 6, 9, 14 mL/s) and ignition delays (0, 10, 20, 30 s). The results suggest that the flame length increased initially with the spread area and reached the maximum at the end of the spreading stage, then followed by a decrease at the shrinking stage and kept nearly constant at the steady stage. For the steady flame length, a new correlation ($L_s/D = 3.1(\dot{Q}^*)^{0.42}$) was established based on dimensionless analysis, which was higher than that for pool fires, highlighting the important differences between spill and pool fires. This developed model was also used to predict the maximum flame length with a maximum deviation of 19.2%, as the heat transfer mechanism and air entrainment are expected to be similar at the shrinking and steady stages. The flame pulsation frequency was determined through the fast Fourier transform (FFT) method, which shows a gradual decrease during the spreading stage while remaining higher than that of pool fires at the steady stage. Subsequently, two new correlations ($f_i = 0.525\sqrt{g/D}$ and $f_s = 0.724\sqrt{g/D}$) were derived from experimental data to predict the pulsation frequency at both spreading and steady stages. The higher frequencies during the steady stage can have a significant influence on the radiation impact to adjacent equipment or personnel. This study not only provides insights into the flame and pulsation behaviors of spill fires but lays a solid foundation for the thermal hazard and risk assessment analysis in the liquid fuel storage and transportation industries.

Keywords: spill fire, flame length, burning area, flame pulsation frequency.

1. Introduction

Liquid petroleum products play a significant role in the energy supply of industrial processes (Betteridge, 2018). Fuel leakage on water is a common accident scenario during marine transportation and spill fire usually occurs after ignition. Whilst spill fires can improve the burning efficiency of the leaked fuel and thus reduce water pollution, it also poses a potential risk for the transportation process and the liquid fuel storage (Roberts, 2004). Different from pool fires, the spread area of spill fires is not confined and as a result the flame length and pulsation behavior could vary greatly with the spread area (Mealy et al., 2014; Hissong, 2007). For example, the Sanchi spill fire accident occurred due to the collision with a cargo ship in East China Sea in 2018. The maximum flame length reached around 800 meters due to the large amount of fuel leakage, which produced a strong radiative heat flux, eventually resulting in the explosion of Sanchi and 32 deaths (Xing et al., 2022). Table 1 presents several other recent continuous spill fires accidents in China, which occurred in the fuel storage and transportation industries with serious consequences. Therefore, it is extremely important to study the flame behavior for spill fires to clarify its accidental hazards and provide protection for industrial safety.

Table 1 Summary of spill fire accidents.

Time	Site	Cause	Consequences	References
2016.4.22	Jingjiang	Tank ignited	Resulting in the burning area of 2000 m^2 and the death of one firefighter.	Hua (2017)
2013.11.22	Qingdao	Pipeline leakage	62 people were killed and 136 were injured.	Liu et al. (2021)
2014.3.1	Jincheng	Tank truck leakage	The spill fire caused 40 deaths, 12 injured and 42 vehicle destroyed.	Ingason and Li (2017)
2010.7.16	Dalian	Pipeline fire	The burning area was close to 60,000 m^2, one firefighter died.	Liu et al. (2021)

In the past decades, extensive research has been conducted on flame behavior, including flame length and flame pulsation frequency (Zukoski et al., 1985; Heskestad, 1981; Fay, 2006; Wang et al., 2023; Shi et al., 2023). Zukoski et al. (1985) examined various experiments with different heat release rates ($\dot{Q}$) and provided a definition for the average flame length, representing the flame length with a 50% probability of occurrence. Heskestad (1981) performed pool fire experiments using different fuels and introduced a dimensionless flame length, determined by the ratio of flame length to burning diameter. Several studies on flame pulsation frequency in pool fires have also been performed (Cetegen and Ahmed, 1993; Zhang et al., 2020; Huang et al., 2021). Cetegen and Ahmed (1993)

systematically investigated the oscillatory phenomenon of diffusion flames through a series of experiments employing round and square burners. They subsequently established a relationship between frequency and burning diameter ($f \sim 1/\sqrt{D}$). This correlation was subsequently used by other scholars (Heskesta, 2016; Zhang et al., 2020; Huang et al., 2021;). Zhang et al. (2020) examined the impacts of restricted conditions (free, wall, and corner flames) with gaseous burners. They observed that free flames exhibited the highest flame pulsation frequency, followed by wall flames, and then corner flames. Huang et al. (2021) performed experiments with varying sizes of sidewalls and discovered that the presence of sidewalls substantially decreased the frequency of flame pulsation by impeding air entrainment. These studies provide clear evidence of the close relationship between flame behaviors (including flame length and pulsation frequency) and factors such as heat release rate, burner diameter, and boundary conditions.

Over the past years, the burning area and flame behavior of spill fires were investigated by some scholars (Li et al., 2017; Mealy et al., 2014; Li et al., 2021). Li et al. (2017) conducted spill fire experiments using a rectangular platform (12 m long) and varying discharge rates (10-40 mL/min). They divided the spill fire development into five stages based on the change in the burning area. In their study, Hasemi's model (originally for rectangular pool fires) was directly used to predict spill fire flame length for thermal hazard calculations. Mealy et al. (2014) performed instantaneous spill fire experiments and observed a linear decrease in flame length with the shrinking burning area. Recently, Li et al. (2021) conducted continuous spill fire experiments with different discharge rates (0.67-6.67 mL/s) and analyzed the fuel spread process. They discovered that the burning area increased again after the shrinking stage due to restricted air entrainment in a tunnel environment. Li et al. (2021) studied flame length in spill fires for different discharge rates (0-500 mL/min) and identified three regimes: increasing, decreasing, and stable, as functions of the discharge rate (Q_{in}). They also obtained the flame pulsation frequency using fast Fourier transform (FFT) and found it to be predominantly influenced by the fuel discharge rate. These studies demonstrate that spill fire flame behaviors are influenced by discharge conditions and the fuel spread process. However, to the best of the authors' knowledge, the detailed flame behaviors of spill fire during the whole spread process have not been investigated in a systematic manner especially with large burner diameters. Furthermore, very few studies have reported the flame pulsation frequency at the spreading stage.

To investigate flame length and pulsation behavior of continuous spill fires on water, large-scale experiments with a pan diameter of 6 m were conducted in this study. Systematic analysis of flame length and pulsation behavior was performed under various experimental conditions. Through dimensionless analysis, a new model for flame length during the steady stage was developed and compared with existing models for pool fires. Additionally, new correlations were proposed for the

flame pulsation frequency during both spreading and steady stages.

2. Experimental setup and methods

2.1. Experimental setup

The experimental setup for continuous spill fires on water is depicted in Fig. 1(a). A circular stainless steel pan with a 6 m diameter was used, as shown in Fig. 1(b). Before the experiments, the pan was filled with water of 25 cm, which was used to simulate the burning fuel on water during firefighting of tank fires or due to leaked fuels on water during transportation. N-heptane was used as fuel as it was also used in previous spill fire studies. A peristaltic pump was used to supply the fuel, which was released from the container onto the water surface at a steady flow rate. A Sartorius balance with an accuracy of 0.1 g was used to measure the residual mass and to ensure the desired discharge rate. More comprehensive experimental details can be found in our previous study in which gasoline was used (Zhao et al., 2022). The flame length and pulsation behavior were recorded using two digital cameras from different perspectives and angles at a frame rate of 25 frames per second. Camera 1 was positioned at a certain angle to capture the spread area, while Camera 2 was placed 15 m away to capture the flame length, enabling the calculation of the flame pulsation frequency.

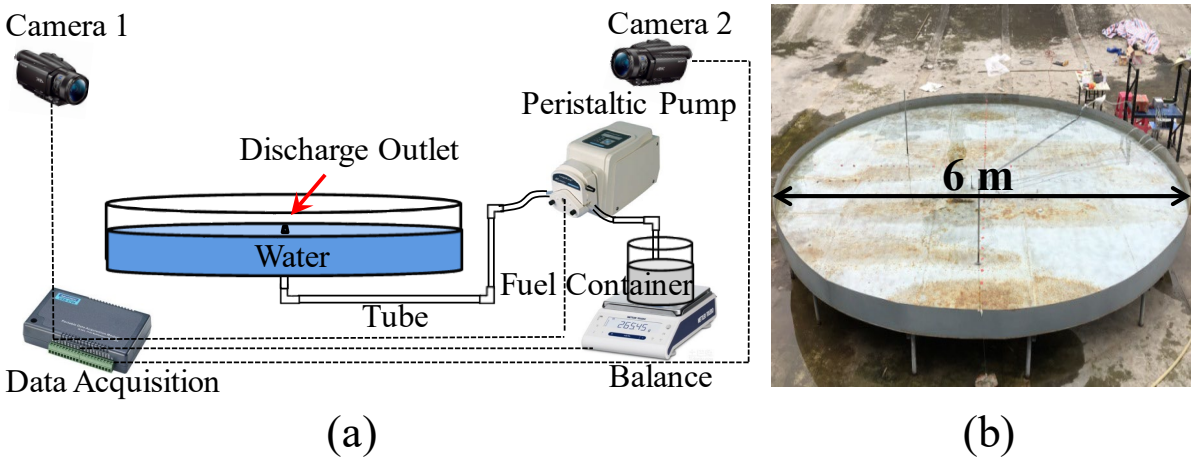

Fig. 1. Experimental arrangement: (a) experimental apparatus; (b) the pan.

All tests were conducted outdoors, and the wind velocity was less than 0.2 m/s, so the effect of the wind could be ignored. To understand the effects of fuel discharge rate and ignition delay (t_s, the time from the fuel release to the ignition) on the flame length and pulsation behavior, 16 tests conditions were considered for four discharge rates (Q_{in} = 3, 6, 9, 14 mL/s) and four ignition delays (t_s = 0, 10, 20, 30 s) as listed in Table 2. At least two tests were conducted for each experimental configuration, and the results showed good repeatability.

Table 2 Summary of the continuous spill fire tests.

Number.	Discharge rate (mL/s)	Ignition delay (s)	Leakage time (s)	Fuel volume (mL)
1	3	0	125	375
2	6	0	125	750
3	9	0	125	1125
4	14	0	125	1750
5	3	10	150	450
6	6	10	150	900
7	9	10	150	1350
8	14	10	150	2100
9	3	20	160	480
10	6	20	160	960
11	9	20	160	1440
12	14	20	160	2240
13	3	30	170	510
14	6	30	170	1020
15	9	30	170	1530
16	14	30	170	2380

2.2. Flame length extraction method

In the experiment, Camera 2 was used to record the burning process and an algorithm was developed to extract flame length (Zhao et al., 2022). The detail picture processing is shown in Fig. 2. First, the color information in the origin image (Fig. 2(a)) was removed, so that the flame is bright enough for further identification. Then, the grayscale image can be obtained as shown in (Fig. 2(b)). Subsequently, the obtained grayscale image was binarized and segmented by setting a threshold to obtain the boundary line of the flame (Fig. 2(c)). During the experiments, it was discovered that setting the threshold value at 8% of the grayscale pixel value was appropriate. By applying this threshold value, a distinct binary image was obtained by delineating the boundary line, and the actual flame length can be calculated accurately using a reference object within the image. Similarly, the instantaneous burning radius was determined from the images captured by Camera 1. Fig. 2(e) depicts the average flame length of a continuous spill fire with a discharge rate of 14.0 mL/s and an ignition delay of 30 s.

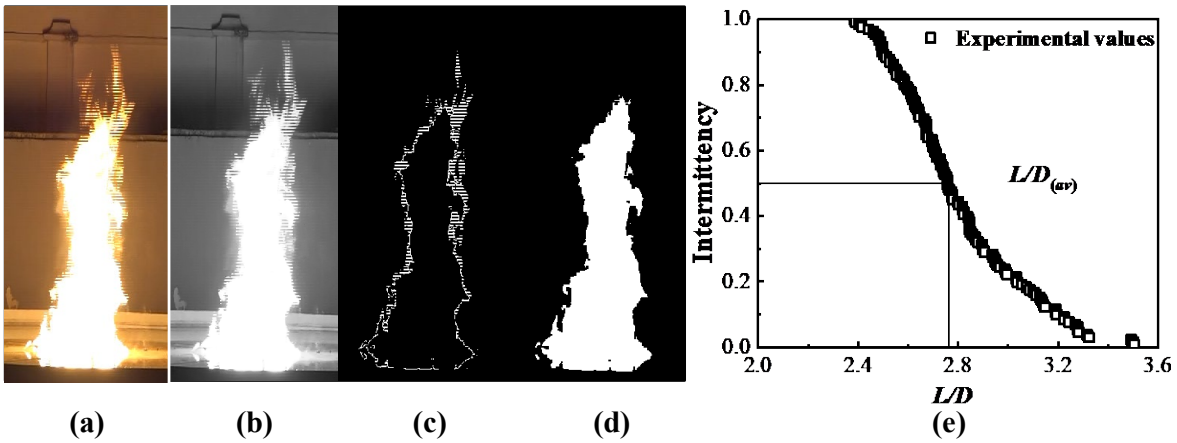

Fig. 2. Flame length extraction process and the mean flame length in Test-16.

2.3. Flame pulsation frequency extraction method

The flame pulsation frequency in spill fires was determined through the application of a fast Fourier transform (FFT) method, similar to the approach used in Tang et al. (2014). The flame frequency was derived by analyzing the temporal changes in the continuous image sequence. Firstly, the sequential flame images were obtained by analyzing videos at 25 frames per second, and each image was processed into a binary image as demonstrated in Fig. 2. Then, every complete oscillation cycle was identified within a certain number of continuous images. Finally, the flame pulsation frequency during one oscillation cycle can be calculated as the time interval between two frames is fixed (i.e., 0.04 s). Fig. 3 presents some typical flame images from one oscillation cycle in Test-16, along with the corresponding calculated flame pulsation frequency.

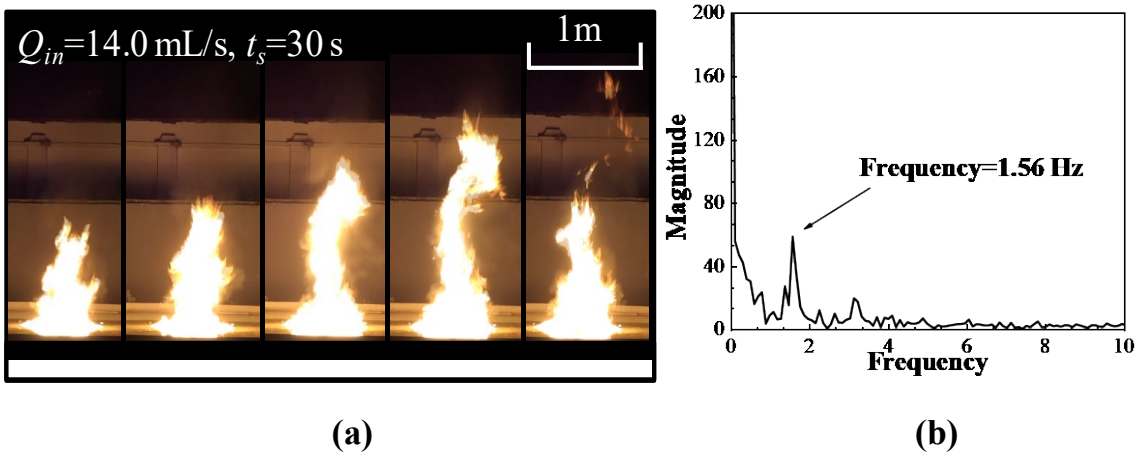

Fig. 3. Typical flame images of the spill fire and the corresponding flame pulsation frequency extraction in Test-16.

3. Results and discussions

3.1. Flame and burning behaviors in the spread process

Upon ignition, the fuel released on the water surface resulted in a rapid propagation of the flame. During this stage, the flame spread over the fuel surface occurred at a significantly faster rate compared to the fuel spread (Li et al., 2017). Fig. 4 shows a series of representative images in Test 4 (Q_{in} = 14.0 mL/s, t_s = 0). Initially, both the flame length and burning area exhibited a rapid increase over time. For example, the flame length increases from 0.81 m at 10 s to 2.53 m at 32 s. After the initial increase, the flame length decreases slightly from 2.53 m at 32 s to 2.17 m at 75 s, which can be attributed to the decreasing burning area resulted from the larger regression rate. During the time interval of 75 to 110 seconds, the flame length maintains a steady state, indicating that the discharge rate is equivalent to the regression rate. Subsequently, once the peristaltic pump is switched off, the flame length rapidly decreases, leading to the extinguishment of the spill fire.

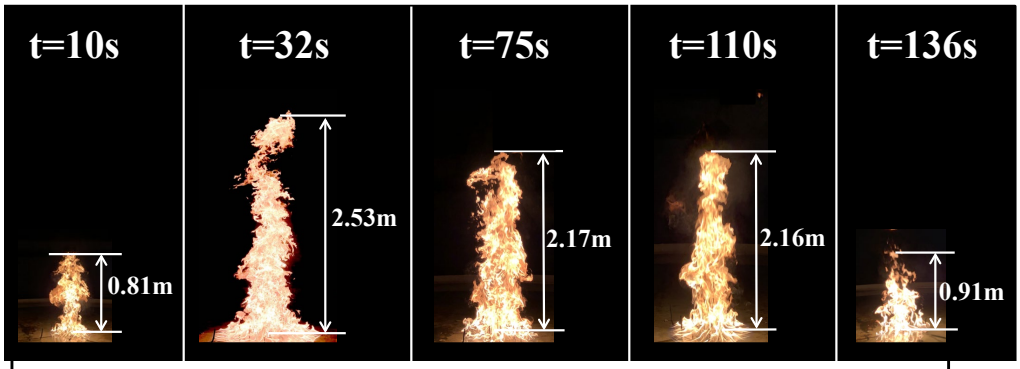

Fig. 4. The typical images of the continuous spill fire in Test 4.

The visual observations in Fig. 4 are also supported by the measured flame length and burning radius shown in Fig. 5 for different discharge rates. The four stages observed in the whole spread process in this study are consistent with the results recorded by Li et al. (2017), named as: 1) spreading, 2) shrinking, 3) steady and 4) extinguishment. The initial growth of flame length can be ascribed to the combined effects of the increasing burning radius influenced by gravity, as depicted in Fig. 5(b), and the intensified heat feedback within the flame. The maximum flame length occurs at the end of the spreading stage, which corresponds to the peak burning area. Subsequently, during the shrinking phase, both the flame length and burning area decrease due to the higher burning rate. This stage is succeeded by a stable stage characterized by nearly constant flame length and burning area, eventually leading to extinguishment.

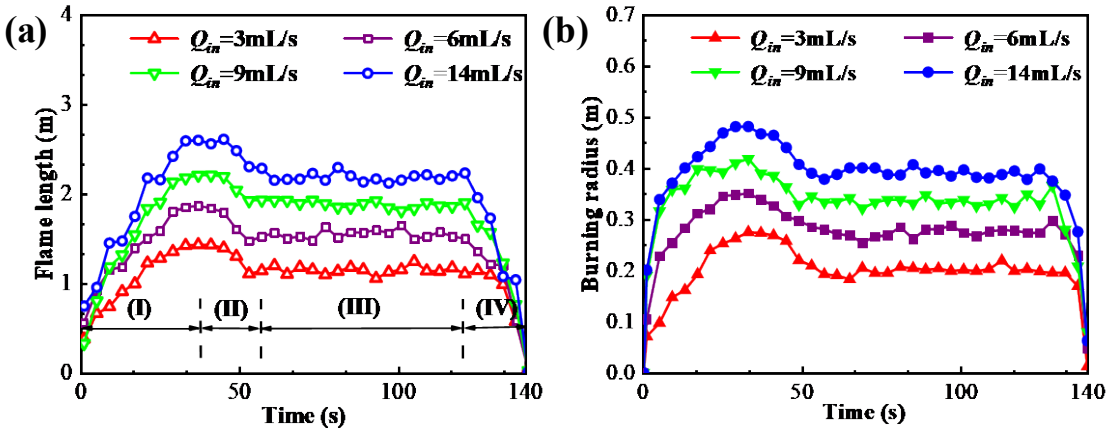

Fig. 5. The variation of (a) flame length and (b) burning radius with time (t_s=0).

As illustrated in Fig. 5, the steady stage of the continuous spill fire sustains for a long time and is therefore closely related to the risk assessment of industrial process. It is widely acknowledged that flame behavior is contingent upon the regression rate (Heskestad, 2016; Zhou et al., 2022). During the steady stage, the burning rate equals to discharge rate (Q_{in}), so:

$$\omega_s = \frac{Q_{in}}{\pi R_s^2} \tag{1}$$

where ω_s is the steady regression rate (m/s), and R_s is the steady burning radius (m).

Table 3 presents a comparison of the steady burning rates observed in spill fires and pool fires at the same burning scales. In continuous spill fires, the burning rate increases with the discharge rate, primarily due to the expansion of the burning radius and the intensified flame radiative heat feedback. Furthermore, the burning rate of spill fires is approximately 0.34 to 0.42 times that of pool fires. This difference arises from the relatively thin fuel layer in spill fires, leading to significant heat transfer to the water below and substantial heat losses to the water layer. Additionally, Table 3 demonstrates that, for a given fuel discharge rate, the ignition delay has a negligible impact on the steady burning area and flame length since both parameters are dependent of the fuel discharge rate. However, the ignition delay does influence the duration required for the spill fire to reach the steady stage.

Table 3 Comparing burning rates: spill fires versus pool fires

Discharge rate, Q_{in} (mL/s)	Ignition delay, t_s (s)	Burning radius, R_s (m)	Burning rate, ω_s (mm/s)	Burning rate, ω_p (mm/s)	ω_s/ω_p
3	0	0.206	0.0225	0.0539	0.417
	10	0.210	0.0216	0.0548	0.394
	20	0.205	0.0227	0.0538	0.422
	30	0.212	0.0213	0.0551	0.387
6	0	0.276	0.0251	0.0673	0.373
	10	0.267	0.0268	0.0658	0.407
	20	0.270	0.0263	0.0663	0.397
	30	0.267	0.0269	0.0657	0.409
9	0	0.327	0.0268	0.0759	0.353
	10	0.317	0.0286	0.0743	0.385
	20	0.313	0.0293	0.0736	0.398
	30	0.322	0.0277	0.0751	0.369
14	0	0.391	0.0291	0.0854	0.341
	10	0.385	0.0300	0.0846	0.355
	20	0.377	0.0314	0.0834	0.376
	30	0.382	0.0306	0.0841	0.364

3.2. Steady flame length

In Fig. 5, the steady burning time of spill fire is relative longer, which mainly determines the fire thermal hazard and the spill fire consequences (Gottuk et al., 2000). Fig. 6 shows the relationship between the steady flame length (L_s) and the burning diameter. It can be observed that the steady flame length exhibits a linear increase with the burning diameter (L_s = 3.07 D-0.25) for continuous spill fires. For comparison, some flame length data from n-heptane pool fires are included in Fig. 6. Evidently, the steady flame length in spill fires is lower than that in pool fires at equivalent burning diameters, with a corresponding ratio ranging from 70.6% to 87.2%. The lower flame length can be attributed to the reduced burning rate in spill fires, as validated in Table 2.

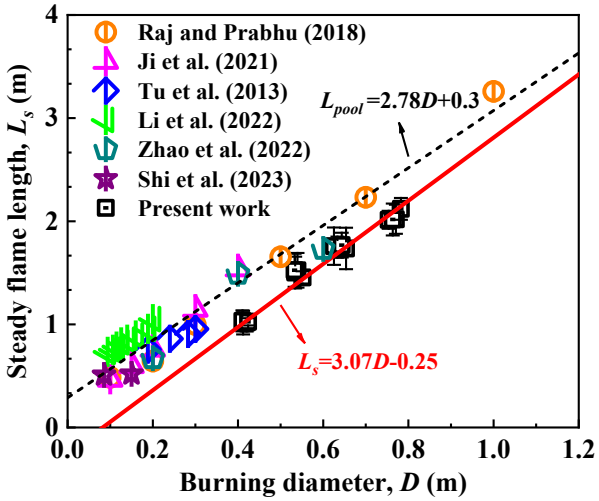

Fig. 6. Comparison of flame length between spill fires and n-heptane pool fires.

The flame length (L_s) observed in continuous spill fires is predominantly influenced by several key factors, including the discharge rate (Q_{in}), burning diameter (D), heat release rate ($\dot{Q}$), burning efficiency (η), and the thickness of the fuel layer (h) (Moorhouse, 1982; Heskestad, 1981), i.e.

$$L_s = fun(Q_{in}, D, \dot{Q}, \eta, h) \tag{2}$$

The dimensionless flame length is commonly correlated to a dimensionless heat release rate $\dot{Q}^*$ (Moorhouse, 1982) as:

$$L_s/D = a(\dot{Q}^*)^b + c \tag{3}$$

where a, b, and c are fitting parameters. The corresponding typical values of pool fires are listed in Table 4, which are mainly determined by the fuel type and burner diameter.

Table 4 The values of the parameters in some pool fire correlations.

Parameters	$\dot{Q}^*$	a	b	c	Note
Heskestad (1983)	$\frac{m'\Delta H_c\pi}{4\rho_\infty c_{pa}T_\infty\sqrt{gD}}$	3.7	0.4	-1.02	turbulent diffusion flames
Mangialavori and Rubino (1992)	$\frac{m'}{\rho_\infty\sqrt{gD}}$	31.6	0.58	0	pool diameter: 1- 6 m
Fay (2006)	$\frac{m'}{\rho_\infty\sqrt{gD}}$	13.8 ± 2.15	2/3	0	LNG pool fires

The dimensionless heat release $\dot{Q}^*$ in the steady stage of spill fires can be calculated as:

$$\dot{Q}^* = \frac{\dot{Q}}{\rho_\infty c_{pa}T_\infty g^{1/2}D^{5/2}} \tag{4}$$

where ρ_∞ is the ambient density, T_∞ is the ambient temperature, g is the gravity acceleration and c_{pa} is the air specific heat. $\dot{Q}$ is the total heat release rate, which can be further expressed as:

$$\dot{Q} = Q_{in}\rho_f H_c \tag{5}$$

where ρ_f is the fuel density, H_c is the combustion heat of heptane.

Fig. 7 presents a comparison of the steady flame length for spill fires and the predicted values from existing pool fire models. It is evident that all the predicted values underestimate the experimental results. This can be attributed to the difference in air entrainment between spill and pool fires. In the case of pool fires, there is stronger air entrainment at the base of the flame due to the presence of sidewall rims (Liu et al., 2020; Zhang et al., 2021). The burning rate around the rim of the pan is lower than the center position, which further enhances air entrainment. In contrast, for spill fires the burning rate at the center is relatively low due to the release of fresh fuel near the discharge point. Fig. 8 provides a schematic representation comparing the air entrainment mechanisms for pool and spill fires.

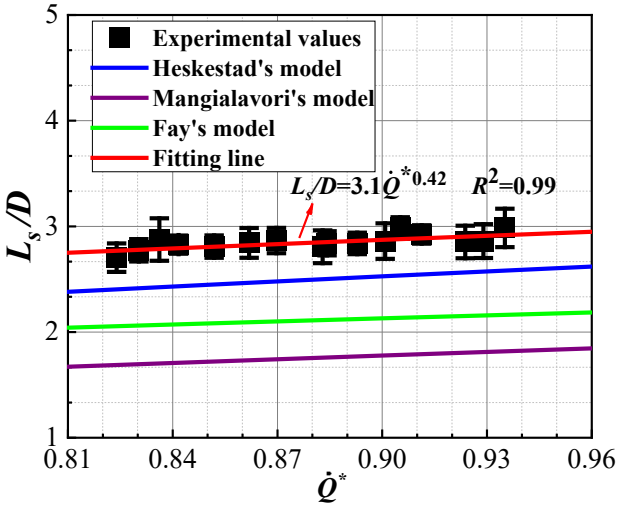

Fig. 7. Comparison between the flame length of spill fires and the predictive values by different models.

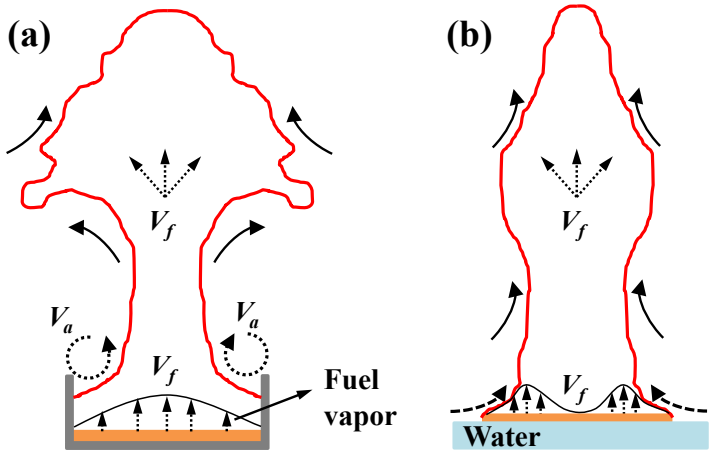

Fig. 8. The air entrainment process for (a) pool fire and (b) spill fire.

Based on the experimental data at the steady stage, the corresponding values of *a* and *b* in Eq. (3)

are 3.1 and 0.42 respectively, so:

$$L_s/D = 3.1(\dot{Q}^*)^{0.42} \tag{6}$$

As illustrated in Fig. 5, both the flame length and burning radius achieve the maximum values at the end of the spreading stage, which correspond to the highest thermal hazard and risk. To estimate the maximum flame length, the burning rate and burning diameter are the key parameters as shown in Eqs. (2-5). The regression rate at the end of the spreading stage (ω_i) can be assumed to be equal to that at the steady stage (ω_s) because of the short duration of the shrinking stage. Hence, the burning rate (m_i') can be expressed as:

$$m_i' = \omega_s \rho_f S_i \tag{7}$$

where S_i is the burning area at the end of the spreading stage.

As the heat transfer mechanism and air entrainment are expected to be similar at the maximum burning radius and steady stage, the flame length model developed for the steady stage (Eq. (6)) is used to estimate the maximum flame length. Fig. 9 displays the dimensionless maximum flame length (L_i/D) for all cases and the corresponding values predicted by Eq. (6). The predictions generally exhibit good agreement with the experimental data, particularly for cases with lower discharge rates. However, for larger discharge rates, the model slightly overestimates the flame length, with a maximum deviation of 19.2%, which could be attributed to the difference in the burning area between the end of the spreading stage and the steady stage, leading to an underestimation of the maximum burning rate. Moreover, the presence of unsteady burning rate and burning area observed in the experiments for higher discharge rates may also contribute to this deviation.

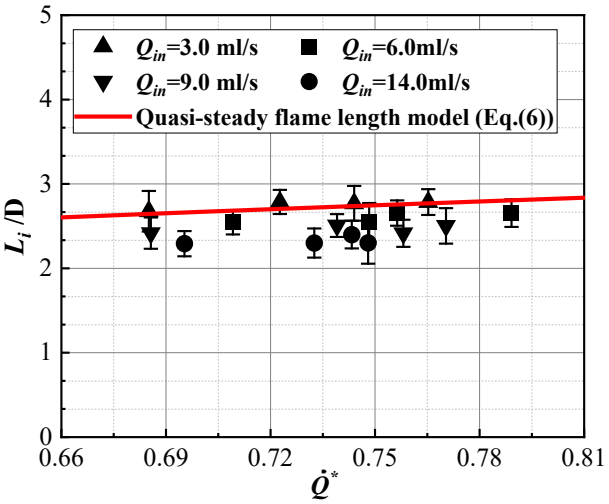

Fig. 9. Comparison between the maximum flame length and the steady flame length model.

3.3. Flame pulsation frequency

The pulsation frequency of a spill fire refers to the frequency of flame pulsations per second during the fuel spread process (Li et al., 2021). In Fig. 10, it can be observed that the flame pulsation frequency (f_i) during the spreading stage gradually decreases over time. This behavior can be explained by considering that the flame pulsation frequency of a buoyant turbulent diffusion flame is primarily influenced by the burning diameter (Cetegen and Ahmed, 1993). As the burning diameter increases during the spreading stage, the air entrainment becomes stronger, leading to an increase in the cycle time for flame pulsation and consequently a decrease in the flame pulsation frequency.

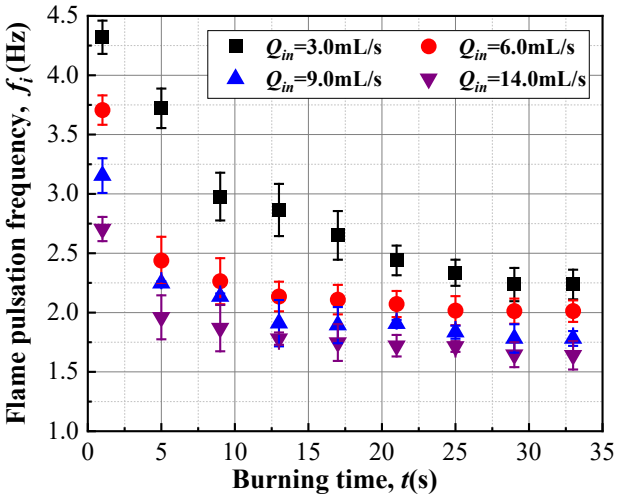

Fig. 10. The flame pulsation frequency in the spreading stage as a function of burning time for Tests 1-4.

For the prediction of the flame pulsation frequency of buoyant diffusion flames, Cetegen and Ahmed (1993) proposed the following formula based on a large number of experiments using propane:

$$f = K\sqrt{\frac{g}{D}}\left[\left(1+\frac{1}{R_i}\right)^{1/2}-\frac{1}{\sqrt{R_i}}\right]^{-1} \tag{8}$$

where $K = C\left(\rho_\infty/\rho_f - 1\right)^{1/2}$, C is a proportionality factor, ρ_∞ is the ambient air density and ρ_f is the source fluid density, K is a constant that needs to be determined by experimental data; g is the gravitational acceleration, and the Richardson number Ri is the ratio of buoyancy force and inertia force:

$$R_i = \frac{(\rho_\infty-\rho_f)gD}{\rho_f u_f^2} \tag{9}$$

where u_f is the bulk velocity of the gas stream at the source.

In the present experiments, u_f is nearly zero so Ri becomes very large. Eq. (8) can be simplified as:

$$f = K\sqrt{\frac{g}{D}} \tag{10}$$

Eq. (10) is commonly used for predicting the pulsation frequency of buoyant diffusion flames (Huang et al., 2021; Zhang et al., 2021). In Fig. 11, the experimental flame pulsation frequency obtained during the spreading stage is compared to previous correlations. The correlation proposed by Cetegen and Ahmed (1993) shows good agreement with the experimental data, though slightly underestimating the flame pulsation frequency for larger values of $\sqrt{g/D}$. The model by Schönbucher et al. (1988) overestimates the pulsation frequency, whereas that by Zukoski et al. (1985) underestimates it. This may be related to the difference in the fuel types and burning scales. By fitting the experimental data, $f_i = 0.525\sqrt{g/D}$ was found for the flame pulsation frequency at the spreading stage (as shown in Fig. 11).

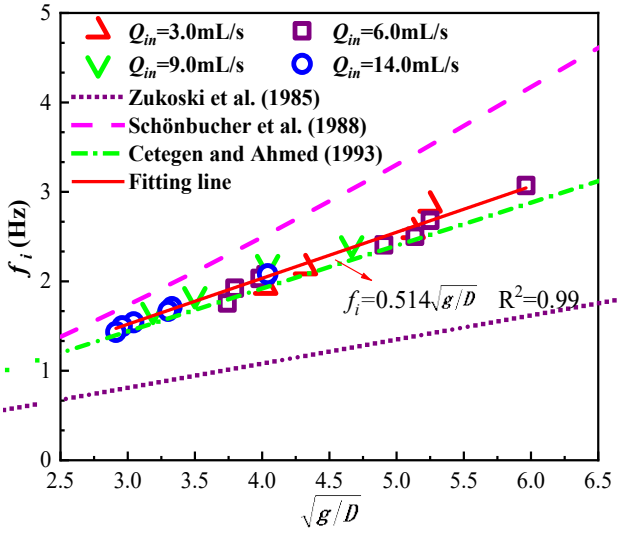

Fig. 11. Comparison between the flame pulsation frequencies at the spreading stage and previous correlations.

Similarly, the flame pulsation frequency (f_s) at the steady stage is depicted in Fig. 12. At a specific discharge rate, the flame pulsation frequency remains relatively consistent, indicating similar burning diameters for the given discharge rate. In addition to this, existing correlations for the flame pulsation frequency of pool fires are presented in Fig. 12 for comparison purposes. It is evident that the flame pulsation frequency of spill fires is consistently higher than that of pool fires for the same $\sqrt{g/D}$. This can be attributed to the stronger air entrainment observed in pool fires due to the presence of sidewalls, resulting in a significant reduction in flame pulsation frequency, as demonstrated in Fig. 8. Compared with the spreading stage, the higher frequencies during the steady stage resulted from the higher burning rate/ heat release rate, which in turn can have a significant influence on the radiation impact to adjacent equipment or personnel and associated thermal hazard and risks analysis in the industrial process. By fitting the experimental values, the correlation $f_i = 0.724\sqrt{g/D}$ has been developed for spill fires at the steady stage.

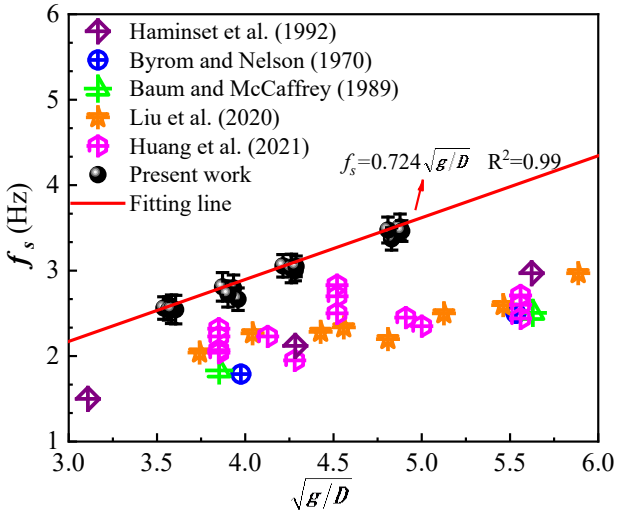

Fig. 12. The comparison of flame pulsation frequency between pool fires and spill fires at the steady stage.

4. Conclusions

This study explores the flame behavior characteristics of continuous spill fires on water. Several spill fire experiments were conducted using n-heptane. Measurements and analysis were performed on the spread area, flame length, and flame pulsation frequency. The following are the main findings:

(1) The flame length is mainly dominated by the spread area for continuous spill fires, exhibiting four distinctive stages: 1) increasing, 2) decreasing, 3) steady, and 4) extinguishment, which coincide with the liquid layer spreading process. The maximum flame length occurs at the end of the increasing stage.

(2) The steady flame length of spill fires is lower than that of heptane pool fires at the same burning scales due to the lower burning rate. A new correlation for the flame length of spill fires was established, using a dimensionless heat release rate ($\dot{Q}^*$) derived from the discharge rate. It is applicable to both steady and maximum flame lengths, with a maximum deviation of 19.2%.

(3) The flame pulsation frequency of continuous spill fires declines with the burning diameter. It increases during the spreading stage and stabilizes during the steady stage. Compared to pool fires, spill fires exhibit a higher flame pulsation frequency at the steady stage due to the lack of sidewall restriction. The respective flame pulsation frequencies for the spreading and steady stages are $f_i = 0.525\sqrt{g/D}$ and $f_s = 0.724\sqrt{g/D}$, respectively.

This study provides a detailed analysis of the flame length and pulsation behaviors for continuous spill fires on a water surface. The increased pulsation frequency during the steady burning stage implies higher radiation impact to adjacent equipment or personnel, so the corresponding risk assessment must be revised accordingly and implemented appropriately. In practical applications, the

findings in this work can also provide guidance for the design of key components and fire extinguishing strategies in chemical industrial parks.

It is worthwhile to note that in a practical accident case the fuel spread process and flame behaviors can be affected by environmental factors (such as wind, and ambient temperature and pressure), fuel type, and burner size. Therefore, to further verify and validate the correlations developed in this work, tests should be conducted for other types of fuels with varying burner sizes and under different atmospheric pressure conditions, which will be addressed in our future studies.

Acknowledgements

This work was sponsored by the National Key R&D Program of China (2022YFC3004900), the Key Research and Development Program of National Fire and Rescue Administration (No. 2022XFZD04), the Fundamental Research Funds for the Central Universities (No. 2020QN05).

References

Baum, H., McCaffrey, B., 1989. Fire induced flow field-theory and experiment. Fire Saf. Sci. 2, 129-148.

Betteridge S., 2018. Modelling large LNG pool fires on water. J. Loss Prev. Process Ind. 56, 46-56.

Byram, G., Nelson, R., 1970. The modeling of pulsating fires. Fire Technol. 102, 102-110.

Cetegen, B.M., Ahmed, T.A., 1993. Experiments on the periodic instability of buoyant plumes and pool fires. Combust. Flame 93 (1-2), 157-184.

Fay, J.A., 2006. Model of large pool fires. J. Hazard. Mater. 136, 219-232.

Gottuk, D., Scheffey, J., Williams, F., Gott, J., Tabet, R., 2000. Optical fire detection (OFD) for military aircraft hangars: final report on OFD performance to fuel spill fires and optical stresses. Naval Research Laboratory, Washington.

Hamins, A., Yang, J., Kashiwagi, T., 1992. An experimental investigation of the pulsation frequency of flames. Symp. (Int.) Combust. 24, 1695-702.

Heskestad, G., 1891. Peak gas velocities and flame lengths of buoyancy-controlled turbulent diffusion flames. Proc. Combust. Inst. 18 (1), 951-960.

Heskestad, G., 1983. Luminous Heights of Turbulent Diffusion Flames. Fire Saf. J. 5, 103-108.

Heskestad, G., 2016. Fire plumes, flame length, and air entrainment. SFPE Handbook of Fire Protection Engineering, Springer.

Hissong, D.W., 2007. Keys to modeling LNG spills on water. J. Hazard. Mater. 140 (3), 465-477.

Hua, B., 2017. Discussion on fire fighting and rescue work based on the explosion and fire accident of Jiangsu Deqiao Warehousing. Ltd in Jingjiang, Taizhou on April 22, China Fire Protection Community 11, 61-62.

Huang, X., Huang, T., Zhuo, X., Tang, F., He, L., Wen, J., 2021, A global model for flame pulsation frequency of buoyancy-controlled rectangular gas fuel fire with different boundaries. Fuel 289, 119857.

Ingason, H., Li, Y., 2017. Spilled liquid fires in tunnels. Fire Saf. J. 91, 399-406.

Ji, J., Ge, F., Qiu, T., 2021. Experimental and theoretical research on flame emissivity and radiative heat flux from heptane pool fires. Proc. Combust. Inst. 38, 4877-4885.

Li, H., Liu, H., Liu, J., Ge, J., Tang, F., 2021. Spread and burning characteristics of continuous spill fires in a tunnel. Tunn. Undergr. Space Technol. 109 , 103754.

Li, M., Han, G., Geng, S., 2022. Experimental study and new-proposed mathematical correlation of flame height of rectangular pool fire with aspect ratio and mass burning rate. Energy 255, 124604.

Li, M., Luo, Q., Ji, J., Wang, C., 2021, Hydrodynamic analysis and flame pulsation of continuously spilling fire spread over n-butanol fuel under different slope angles. Fire Saf. J. 126 , 103467.

Li, Y., Huang, H., Wang, Z., Zhang, J., Jiang, C., Dobashi, R., 2015. An experimental and modeling study of continuous liquid fuel spill fires on water. J. Loss Prev. Process. Ind. 33, 250-257.

Li, Y., Huang, H., Zhang, L., Su, B., Zhao, J., Liu, Q., 2017. An experimental investigation into the effect of substrate slope on the continuously released liquid fuel spill fires. J. Loss Prev. Process Ind. 45, 203-209.

Liu, C., Ding, L., Jangi, M., Ji, J., Yu, L., Wan, H., 2020. Experimental study of the effect of ullage height on flame characteristics of pool fires. Combust. Flame 216, 245-255.

Liu, J., Li, D., Wang, Z., Chai, X., 2021 A state-of-the-art research progress and prospect of liquid fuel spill fires. Case Stud. Therm. Eng. 28, 101421.

Mangialavori, G., Rubino, F., 1992. Experimental tests on large hydrocarbon pool fires. 7th International Symposium on Loss Prevention and Safety Promotion in the Process Industries Taormina, Italy, 4-8.

Mealy, C., Benfer, M., Gottuk, D., 2014. Liquid Fuel Spill Fire Dynamics. Fire Technol. 50, 419-436.

Moorhouse, J., 1982. Scaling criteria for pool fires derived from large scale experiments. The Assessment of Major Hazards, Symposium Series, 71, 165-179.

Raj, V.C., Prabhu, S.V., 2018. Measurement of geometric and radiative properties of heptane pool fires. Fire Saf. J. 96, 13-26.

Roberts T.A., 2004. Linkage of a known level of LPG tank surface water coverage to the degree of jet-fire protection provided. J. Loss Prev. Process Ind. 17 (2), 169-178.

Schönbucher, A., Arnold, B., Banhardt, V., Bieller, V., Kasper, H., Kaufmann, M., Lucas, R., Schiess, N., 1988. Simultaneous observation of organized density structures and the visible field in pool

fires. Symp. (Int.) Combust. 21, 83-92.

Shi, C., Deng, L., Ren, F., Tang, F., 2023. Experimental study on the flame length evolution of two adjacent hydrocarbon pool fires under transverse air flow. Energy 262, 125520.

Tang, F., Hu, L., Wang, Q., Ding, Z., 2014. Flame pulsation frequency of conduction-controlled rectangular hydrocarbon pool fires of different aspect ratios in a sub-atmospheric pressure. Int. J. Heat Mass Transf. 76, 447-451.

Tu, R., Fang, J., Zhang, Y., Zhang, J., Zeng, Y., 2013. Effects of low air pressure on radiation-controlled rectangular ethanol and n-heptane pool fires. Proc. Combust. Inst. 34, 2591-2598.

Wang, T., An, W., Experimental study on flame spread and extinction over horizontal power cables under longitudinal ventilation in a utility tunnel. Therm. Sci. Eng. Prog. 39 (2023), 101752.

Xing, W., Zhu, L., 2022. Assessing the impacts of Sanchi incident on Chinese law concerning ship-source oil pollution. Ocean Coastal Manage. 225, 106227.

Zhang, X., Fang, X., Hu, L., 2021. Buoyant turbulent diffusion flame lengths of free-, wall- and corner air entrainment conditions: experiments and global model based on mirror approach, Fuel 303, 121338.

Zhang, X., Fang, X., Miao, Y., Hu, L., 2020. Experimental study on pulsation frequency of free-, wall- and corner buoyant turbulent diffusion flames. Fuel 276, 118002.

Zhao, J., Song, G., Zhang, X., Li, Y., Zhang, J., Yang, R., 2022. Experimental investigation and modeling of the spread and burning behaviors of continuous spill fires on a water surface. Process Saf. Environ. Prot. 168, 88-95.

Zhao, J., Zhang, X., Zhang, J., Wang, W., Chen, C., 2022. Experimental study on the flame length and burning behaviors of pool fires with different ullage heights. Energy 246, 123397.

Zhao, K., Wang, Z., Ma, S., Ju, X., Guo, P., Cao, X., 2022. Experimental study on the diffusion burning and radiative heat delivery of two adjacent heptane pool fires. Int. J. Therm. Sci. 171, 107246.

Zhou, Y., Xu, B., Zhang, X., Yang, Y., 2022. A comparative study on horizontal flame spread behaviors of thermoplastic polymers with different melt flow indexes under external radiation. Therm. Sci. Eng. Prog. 35, 101463.

Zukoski, E.E., Cetegen, B.M., Kubota, T., 1985. Visible structure of buoyant diffusion flames. Proc. Combust. Inst. 20 (1), 361-366.